MITSUBISHI ELECTRIC RESEARCH LABORATORIES
https://www.merl.com

Modeling, Simulation and Control of Turboelectric Propulsion Systems for More Electric Aircrafts using Modelica

de Castro, Marcelo; Wang, Yebin; Vanfretti, Luigi; Wang, Hongyu; Liu, Dehong; Bortoff, Scott A.; Takegami, Tomoki

TR2022-087 August 06, 2022

Abstract

As industry moves towards More Electric Aircraft technologies, electrification of non- propulsive loads is becoming more common. Moreover, new designs for electrified propulsive systems have been proposed in the literature, drawing attention from the aviation sector. Amidst the proposed topologies, turboelectric architectures present a set of benefits, becoming attractive for more electric powertrains. Given this context, this current paper presents Modelica as the means for developing models to assess the dynamic performance for the different possible turboelectric architectures that can be adopted by industry in the next few years. Individual components have their mathematical models presented along with their respective Modelica implementation. Two different possible architectures are assembled using the Modelica models and their dynamic performances over a 400-second sample flight mission are assessed. The dynamic simulations provide insights for choosing system's parameters, controllers' design, and system sizing.

AIAA Aviation Forum 2022

Mitsubishi Electric Research Laboratories, Inc.
201 Broadway, Cambridge, Massachusetts 02139

Modeling, Simulation and Control of Turboelectric Propulsion Systems for More Electric Aircrafts using Modelica

Marcelo de Castro*, Luigi Vanfretti †
Rensselaer Polytechnic Institute, Troy, NY, 12180

Yebin Wang ‡, Hongyu Wang§, Dehong Liu ¶, Scott Bortoff ‖
Mitsubishi Electric Research Laboratories, Cambridge, MA, 02139

Tomoki Takegami**
Mitsubishi Electric Corporation, Amagasaki City, Japan

As industry moves towards More Electric Aircraft technologies, electrification of non-propulsive loads is becoming more common. Moreover, new designs for electrified propulsive systems have been proposed in the literature, drawing attention from the aviation sector. Amidst the proposed topologies, turboelectric architectures present a set of benefits, becoming attractive for more electric powertrains. Given this context, this current paper presents Modelica as the means for developing models to assess the dynamic performance for the different possible turboelectric architectures that can be adopted by industry in the next few years. Individual components have their mathematical models presented along with their respective Modelica implementation. Two different possible architectures are assembled using the Modelica models and their dynamic performances over a 400-second sample flight mission are assessed. The dynamic simulations provide insights for choosing system's parameters, controllers' design and system sizing.

I. Nomenclature

GHG	=	Greenhouse Gas
MEA	=	More Electric Aircraft
EAP	=	Electrified Aircraft Propulsion
BLI	=	Boundary Layer Injection
$PMSG$	=	Permanent Magnet Synchronous Generator
$FCSG$	=	Field Controlled Synchronous Generator
$PMSM$	=	Permanent Magnet Synchronous Motor
AC	=	Alternating Current
DC	=	Direct Current
MSL	=	Modelica Standard Library
VSC	=	Voltage Source Converter
CSD	=	Constant Speed Drive
$VSVF$	=	Variable Speed Variable Frequency
VSI	=	Voltage Source Inverter
rpm	=	Rotations Per Minute

*Doctorate Candidate, Department of Electrical Computer and Systems Engineering, Rensselaer Polytechnic Institute
†Associate Professor, Department of Electrical Computer and Systems Engineering, Rensselaer Polytechnic Institute.
‡Senior Principal Research Scientist, Multi-Physics & Dynamics Group, Mitsubishi Electric Research Laboratories.
§Visiting Research Scientist, Multi-Physics & Dynamics Group, Mitsubishi Electric Research Laboratories.
¶Senior Principal Research Scientist, Multi-Physics & Dynamics Group, Mitsubishi Electric Research Laboratories.
‖Strategic Project Leader and Chief Scientist, Multi-Physical Systems Group, Mitsubishi Electric Research Laboratories.
**Advanced Technology R&D Center, Mitsubishi Electric Corporation

II. Introduction

A. Background

INCREASING growth in global environmental concerns have made it evident that substantial cuts in Greenhouse Gas (GHG) emissions from the transportation sector are needed. In this context, the aviation industry, being a large contributor to these emissions, has continuously developed advanced energy-efficient solutions to diminish its environmental impact. In fact, important progress has been made in the aviation sector during the past decades to move towards More Electric Aircraft (MEA) designs [1].

The main goal of moving into MEAs is to transform any non-propulsive load in an airplane to be fed by the electrical power system of the aircraft. Increasing aircraft electrification is envisioned to bring in benefits such as higher efficiency, controllability and reconfigurability to the aircraft's components, while facilitating maintenance procedures [2]. This set of advantages is easily translated into economic benefits.

In addition to electrification of non-propulsive loads, different architectures for Electrified Aircraft Propulsion (EAP) systems have been proposed in the literature [3, 4]. Among the different proposed propulsion systems turboelectric architectures have been drawing attention due to many factors. When alone, turboelectric propulsion systems are less efficient than conventional configurations. However, they can be combined with Boundary Layer Ingestion (BLI) and distributed propulsion systems in order to create highly energy efficient configurations [5].

In the BLI design the jet and wake are located in the same axis, resulting in less noise and weight and, consequently, increasing the aircraft's energy efficiency [4]. Hence, a turboelectric architecture strikes a nice balance between fuel burn reduction, power/energy density, and technological readiness level, hence becoming the most attractive topology for more electric powertrains [6].

A general turboelectric propulsion system configuration of an MEA is depicted in Figure 1. Note that the structure allows for the generator to be indirectly connected to the motor, meaning that the two AC systems have certain independent controls and resulting in increased operation flexibility overall. However, there are plenty different ways to assemble the AC/DC/AC system, depending on many aspects of the AC/DC/AC system.

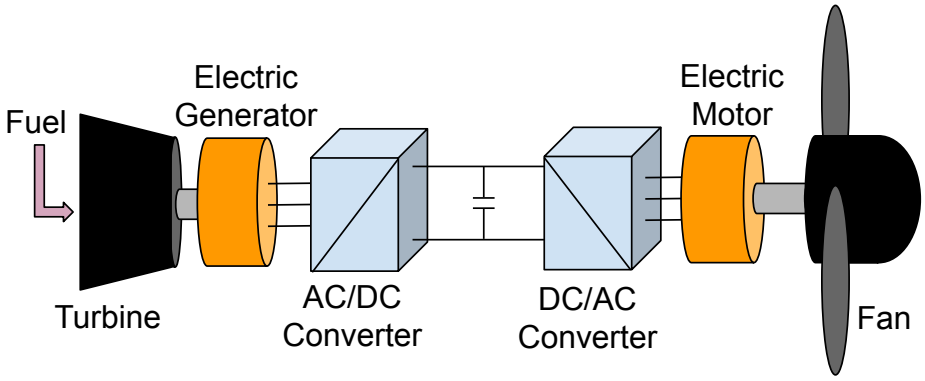

Fig. 1 General architecture for a full turboelectric propulsion system.

At the component level, for example, different types of components can be integrated to fulfill the functionality of the electric propulsion branch: delivering electric propulsive power. For instance, AC power sources, such as a Field Controlled Synchronous Generator (FCSG) or a Permanent Magnet Synchronous Generator (PMSG), can be used as a generation unit. At the load side, synchronous reluctance machine, induction machine, or Permanent Magnet Synchronous Motor (PMSM), etc. can be used. Without loss of generality, in this study, the electric motor is always considered to be the PMSM, due to its higher efficiency and power density if compared to other alternatives such as induction motors [1].

At the system level, the turboelectric architecture allows the generator to be indirectly connected to the motor through controllable power electronics. However, there are a plenty of different ways to assemble the AC-to-DC-to-AC system depending on the type of power electronics used to perform AC/DC and DC/AC conversions. By investigating different design options, rules of thumb to guide the system integration process could be established, helping engineers in the design process of turboelectric propulsion systems.

Hence, the turboelectric architecture depicted on Figure 1, although seemingly simple, offers a variety of design

options and it is worthwhile exploring distinctive design options of architectures and understanding their pros and cons. The different configurations together with some parameter values are determined in a 0-D sizing procedure which is not covered in this particular paper.

In model-based design paradigm, the dynamics of Electric Power System (EPS) are modeled and simulated for evaluation in both steady state and transient behavior, and Modelica solutions are one of the main alternatives for the modeling and simulation of MEA's EPS [1, 7]. Modelica is an equation-based object-oriented language that allows the representation of dynamic systems without a specific direction for the flow of information. The model, which is decoupled from the solver, is automatically compiled into C code and then executed by the computer [8]. The resultant a-causal model has a relatively small amount of algebraic loops, allowing the systems to be simulated more efficiently.

Due to these rich features, the different studied systems in this paper are assembled using Modelica language. The component models that are used to assemble the different turboelectric architectures are especially developed for this task. In addition, because EPS involves multiple time scales and heavy computation in simulation validation, special care should be exerted during the development of system model and the selection of simulation platform. In this study, the $dq-$frame modeling approach is adopted for simulation efficiency [2].

B. Goals and Objectives

Given this context, the present study serves a three-fold purpose:

1) to develop Modelica models and simulation packages to facilitate the analysis of turboelectric propulsion systems;
2) to assess the dynamic performance, also known as 1-D assessment, of different turboelectric propulsion architectures using the developed Modelica models; and
3) to assess Modelica as a tool for assessing different turboelectric architectures while presenting the implementation of the component models.

C. Paper Organization

The remainder of this paper is organized as follows: Sections III and IV present the mathematical formulation and Modelica implementation of the different models representing machines and power electronic converters, respectively, which are used to compose the studied turboelectric architectures. Section V presents the control strategies that are used in the different systems assessed. Section VI presents the modeling of the flight mission as a load curve to the studied turboelectric propulsion system. Section VII depicts the different studied systems which are implemented in a digital simulation environment, while Section VIII present relevant simulation results. Final discussion and concluding remarks are presented in Section IX.

III. Modeling and Implementation of Electrical Machines

In this section, the mathematical models in $dq-$frame are described for the electromechanical components that are needed for assembling the different architectures that are assessed in this paper. They are used to represent the electrical generator and motor that are part of the turboelectric architecture that is presented in Figure 1. In addition to the specific set of differential equations that govern their dynamic behavior, their Modelica implementation is also shown.

A. Permanent Magnet Synchronous Motor

The terminal voltages v_{dq0} in the Park reference frame for a surface-mounted In the Permanent Magnet Synchronous Motor (PMSM) are described in Equation (1) [2].

$$\begin{cases} v_d &= R_s i_d - \omega_e \lambda_q + \dfrac{d}{dt}\lambda_d, \\ v_q &= R_s i_q + \omega_e \lambda_d + \dfrac{d}{dt}\lambda_q, \\ v_0 &= R_s i_0 + \dfrac{d}{dt}\lambda_0. \end{cases} \tag{1}$$

where R_s represents the winding resistance, $\omega_e = 2\pi f_e$ is the electrical angular speed, i_{dq0} are the $dq0-$currents flowing into the machine and λ_{dq0} are the flux linkages for $dq0-$axes, which are defined by the Equation (2). Recall that mechanical speed and the electrical speed are proportional as in $\omega_e = p\omega_m$, where ω_m is the mechanical speed and p is the number of pole pairs of the machine.

$$\begin{cases} \lambda_d &= (L_{md} + L_{ls})\, i_d + \lambda_m = L_d i_d + \lambda_m, \\ \lambda_q &= \left(L_{mq} + L_{ls}\right) i_q = L_q i_q, \\ \lambda_0 &= L_{ls} i_0 = L_0 i_0. \end{cases} \tag{2}$$

where λ_m is the magnetic flux coming from the permanent magnet, $L_{m,dq}$ are the $dq-$axes magnetizing inductance values and L_{ls} are the leakage inductance. In addition to that, the mechanical equation is defined by

$$J\frac{d}{dt}\omega_m = T_e - T_L = \frac{3}{2}p\left[\lambda_m i_q + (L_d - L_q) i_d i_q\right] - T_L, \tag{3}$$

where J is the total moment of inertia of the motor, T_e is the electrical torque, T_L is the mechanical load torque and ω_m is the shaft's mechanical speed. The Modelica model of the PMSM can be separated into two parts: the electrical and the mechanical. The former can be declared in form of equations as shown below.

Listing 1 Modelica equations for the electrical part of the PMSM model.

```
equation
  vd = v_d.v - ground.v "Measuring d-voltage";
  vq = v_q.v - ground.v "Measuring q-voltage";
  v0 = v_0.v - ground.v "Measuring 0-voltage";
  iq = v_q.i "Measuring q-current";
  id = v_d.i "Measuring d-current";
  i0 = v_0.i "Measuring 0-current";
  ground.i = v_q.i + v_d.i + v_0.i "Connecting ground current";
  vd = Rs*id - p*measured.w*Lambda_q + der(Lambda_d) "d-voltage equation";
  vq = Rs*iq + p*measured.w*Lambda_d + der(Lambda_q) "q-voltage equation";
  v0 = Rs*i0 + der(Lambda_0) "0-voltage equation";
  Lambda_d = Ld*id + Lambda_m "d-flux linkage equation";
  Lambda_q = Lq*iq "q-flux linkage equation";
  Lambda_0 = L0*i0 "0-flux linkage equation";
  Te = (3/2)*p*(Lambda_m*iq + (Ld - Lq)*id*iq) "Electrical torque";
```

The mechanical equations can be declared in the PMSM model by the use of rotational mechanical components from the Modelica Standard Library (MSL). The electrical torque T_e acts in a rotational body with the motor's moment of inertia as it is shown in Figure 2. The connector named Flange A can then be connected to another mechanical device that will produce the torque on the opposing direction, such as the Fan depicted in Figure 1.

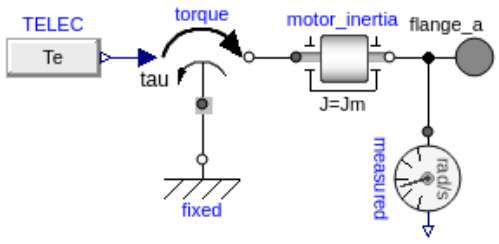

Fig. 2 Modelica diagram for the mechanical equations of a PMSM.

B. Permanent Magnet Synchronous Generator

The PMSG has a similar structure if compared to the PMSM. In fact, if the currents are considered to be entering the generator's terminal, then (1) are the same in PMSG equations. The difference is that a generator takes the energy

from the shaft and transforms it into electrical energy. This energy flow ends up causing the electromechanical swing equation to be written as

$$J\frac{d\omega_m}{dt} = T_G - T_e = T_G - \frac{3p}{2}\left(\lambda_q i_d - \lambda_d i_q\right) \tag{4}$$

where T_G is the torque applied in the shaft by the generator's primary machine. Therefore, the Modelica model representing the electrical circuit is the same as the one shown in Listing 1 and the only difference between the PMSG and the PMSM would be the implementation of the swing equation, resulting in a slightly different diagram as the one shown in Figure 2. In fact, in the generator, instead of `Te` one would find `-Te`.

C. Field Controlled Synchronous Generator

Another possible configuration for a synchronous generator is based on the magnetic field being generated by an external circuit which allows the excitation to be controlled. The simplified circuits for both d and q axes, with their respective damping windings, can be drawn as shown in Figure 3 [2]. Note that the field circuit appears on the left-hand side of the d-axis circuit and, by controlling that voltage source, the current i_f allows control over an excitation flux, enabling the regulation of terminal voltage by control of d-axis component of voltage.

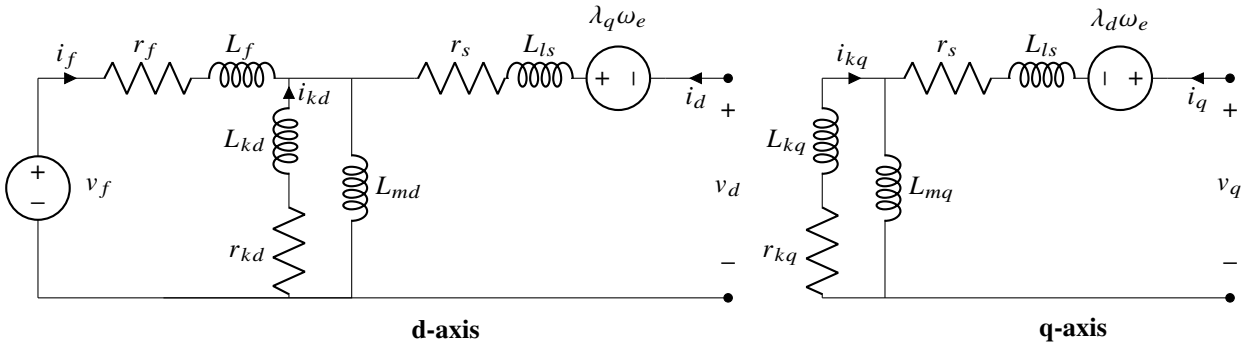

Fig. 3 Diagram representation for the dq-axis' electrical circuits of the FCSG model that is used in this study.

From Fig. 3, if the d-axis circuit is divided into two loops it is possible to derive the differential set of equations presented in 5.

$$\begin{cases} v_f &= r_f i_f + L_f \dfrac{d}{dt} i_f + L_{md}\dfrac{d}{dt}(i_d + i_f + i_{kd}), \\ v_d &= -\omega_e \lambda_q + r_s i_d + L_d \dfrac{d}{dt} i_d + L_{md}\dfrac{d}{dt}(i_f + i_{kd}), \\ v_q &= \omega_e \lambda_d + r_s i_q + L_q \dfrac{d}{dt} i_q + L_{md}\dfrac{d}{dt} i_{kd}. \end{cases} \tag{5}$$

where $L_q = L_{ls} + L_{mq}$ and $L_d = L_{ls} + L_{md}$. In addition, the fluxes are

$$\begin{cases} \lambda_d = L_d i_d + L_{md}(i_f + i_{kd}), \\ \lambda_q = L_q i_q + L_{md} i_{kq}. \end{cases} \tag{6}$$

In addition to the circuit equations, the swing equation for the FCSG model is the same as the one shown in Eq. (4). The only difference would be the fluxes λ_d and λ_q which are calculated differently depending on the generator model being analyzed. In order to show the versatility of the Modelica language, the FCSG model representation is is built exploring the electrical components available in the Modelica Standard Library (MSL), as depicted in Figure 4. However the diagram might appear completely sufficient in describing the FCSG model, it is also important to present the equations that are written in the `Text` layer of the model. As one can see in Listing 2, the electrical torque as well as the electromagnetic fluxes are all calculated in that layer of the model.

Listing 2 Modelica equations for the FCSG model.

```
equation
  v_0.v = 0 "voltage in 0-sequence";
  we = p * measured.w "electrical frequency";
  iq = v_q.i "Measuring q-current";
  id = v_d.i "Measuring d-current";
  ikq = -damp_Lkq.i "Measuring damping q-current";
  ikd = -damp_Lkd.i "Measuring damping d-current";
  ifd = Efd_p.i "Measuring ifd current";
  lambdaQ = Lq * iq + Lmq * ikq "Induced q-axis magnetic flux";
  lambdaD = Ld * id + Lmd * (ifd + ikd) "Induced d-axis magnetic flux";
  emf_q = lambdaQ * we "Induced q-axis volage";
  emf_d = lambdaD * we "Induced d-axis volage";
  Te = 3 / 2 * p * (lambdaQ * id - lambdaD * iq) "Electrical torque";
```

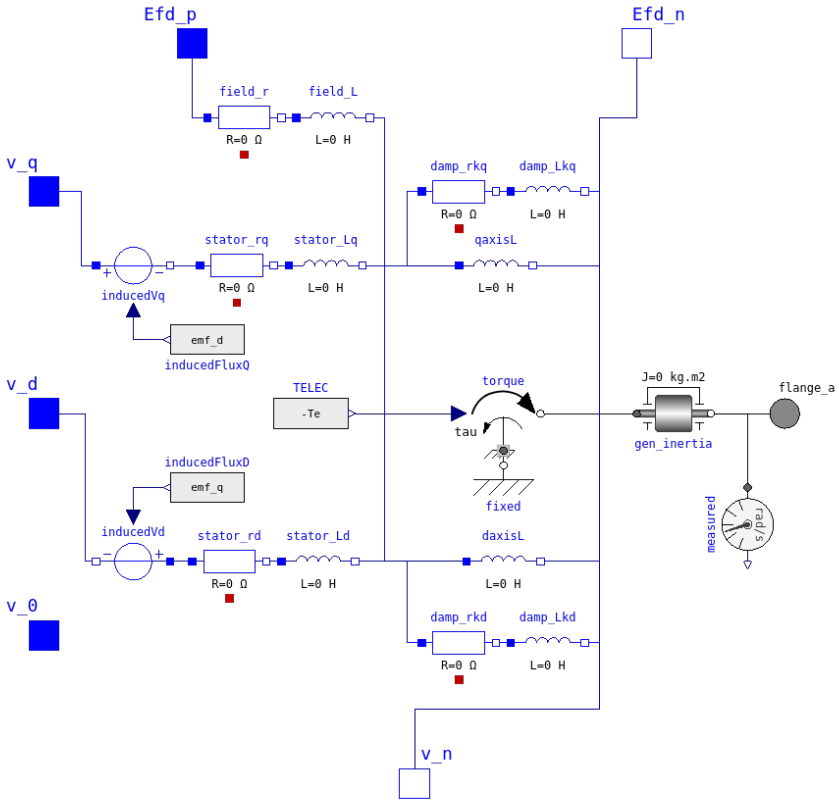

Fig. 4 Modelica diagram for the Field Controlled Synchronous Generator (FCSG) with damping windings.

IV. Modeling and Implementation of Power Electronic Converters

In this section, the Power Electronic Converters (PECs) which are used to interface the AC and DC systems are presented, together with their mathematical model and the respective Modelica implementation. Two converters are modeled here, the Voltage-Sourced Converter (VSC) and the 6-pulse diode bridge. The former can act as both rectifier and inverter while the latter can only be used as a three-phase rectifier. In addition, since all the machines are modeled in the dq-frame, and control strategies for the converters can be more easily implemented when in the $dq-$frame [9], the converters in this study are also modeled in that reference frame.

A. Voltage-Sourced Converters

One common architecture of a VSC can be the two-level converter, which is composed of three half-bridge converters, one for each phase [9]. The converter's switching device is a full-controllable bi-directional cell composed of an IGBT connected in anti-parallel with a diode [9]. The full-switching model of a three-phase VSC can be averaged and then converted to the $dq-$frame by Clarke-Park transformation, yielding Equations (7) [9], which describes the converter's terminal voltage and the DC current relationship with the modulation indices. If the converter is connected using the full-bridge architecture, i.e. there is no mid-point access in the DC bus, equations are slightly different and $\frac{V_{DC}}{2}$ would be replaced by $\frac{V_{DC}}{\sqrt{3}}$.

$$\begin{cases} v_{T,q}(t) &= \dfrac{V_{DC}}{2} m_q(t), \\ v_{T,d}(t) &= \dfrac{V_{DC}}{2} m_d(t), \\ I_{DC}(t) &= -\dfrac{3}{2V_{DC}} \left(v_{T,q} i_q + v_{T,d} i_d \right) = -\dfrac{3}{4} \left(m_q i_q + m_d i_d \right). \end{cases} \tag{7}$$

where $v_{T,dq}$, m_{dq} and i_{dq} are the converter's terminal phase voltages, modulation indices and terminal phase currents in dq coordinates, respectively. Moreover, V_{DC} and I_{DC} are the DC bus voltage and current respectively. Using all these equations and assuming $v_{T,0} \equiv 0$, it is possible to draw an implementation in Modelica that will look like Figure 5. The heat port shown in red, can be used to represent the thermal losses that can be connected to create a thermal representation of the entire electromechanic circuit.

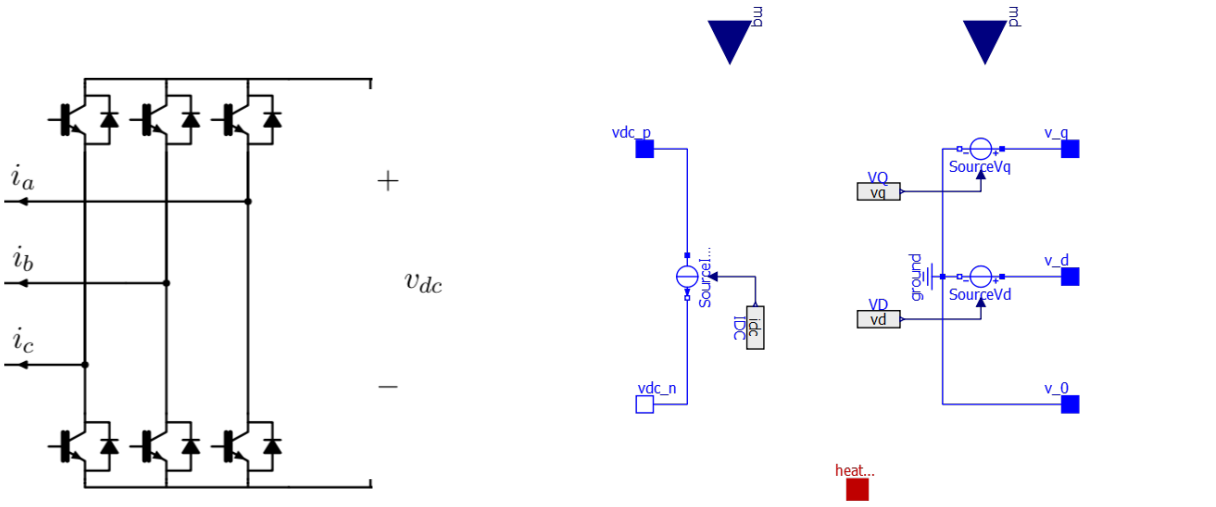

(a) Diagram representing a three-phase VSC. **(b) Averaged implementation of the dq VSC in Modelica.**

Fig. 5 A comparison between the three-phase VSC diagram in abc-frame and its dq-frame implementation in Modelica

Because of the full controllability feature, this converter can be associated with permanent magnet machines in order to allow for the regulation of important variables. When performing DC-to-AC transformation, this converter can be use to control the electric motor's torque and speed, for example. On the other hand, when performing AC-to-DC transformation, this converter can be associated with the PMSG, regulating the reactive power on the generator along with the DC bus voltage.

B. Six-Pulse Diode Bridge Rectifier

The six-pulse bridge, when assembled using diodes as its building blocks, is an uncontrollable rectifier, meaning that its output DC bus voltage is a direct consequence of the voltage waves' amplitude on its AC terminal. This is due to the fact that the diode is an uncontrollable semiconductor device, meaning that the current flowing through it, i_D and the voltage over it, v_{AK}, cannot be controlled by an external device. In fact, these two variables have their behavior completely determined by the polarity of its current and voltage [10].

Given this fact, the relationship between AC voltage amplitude and the DC bus voltage output can b simplified to a simple gain. Since the AC terminal is modeled using dq-frame coordinates and assuming that a invariant-amplitude Park transformation is used [9], then it is possible to write Eq. (8) [11].

$$V_{DC} = \frac{3\sqrt{3}}{\pi}\sqrt{v_d^2 + v_q^2}, \tag{8}$$

where v_{dq} are the dq-frame components of the voltage waves in the rectifier's AC terminal. Moreover, the AC currents resulting from this transformation would be in-phase with respective AC voltages, meaning that the Park reference-frame transformation angle, θ_{dq}, used in voltage variables would also be used in the current variable. In addition, it is necessary to find the peak wave amplitude, in order to calculate the resulting dq-frame values for the current. This is done by simple multiplication as shown in Equation (9) [11].

$$\begin{cases} i_q = \dfrac{2\sqrt{3}}{\pi} I_{DC} \sin\theta_{dq}, \\ i_d = \dfrac{2\sqrt{3}}{\pi} I_{DC} \cos\theta_{dq}. \end{cases} \tag{9}$$

where I_{DC} is the magnitude of the stationary current flowing in the DC terminal of the converter. This set of equations can be implemented in Modelica following what is shown on listing 3.

Listing 3 Modelica equations for the a Park frame six-pulse diode bridge rectifier.

```
equation
  vq = v_q.v - v_0.v "measuring q-axis voltage";
  vd = v_d.v - v_0.v "measuring d-axis voltage";
  Vdc = dc_p.v - dc_n.v "measuring dc-bus voltage";
  dc_n.v = 0 "setting voltage reference";
  vdq = sqrt(vd ^ 2 + vq ^ 2) "voltage magnitude";
  theta = asin(vd/vdq) "Park frame transformation angle";
  Idc = dc_p.i "measuring dc-bus current";
  iq = v_q.i "stating q-axis current";
  id = v_d.i "stating d-axis current";
  i0 = v_0.i "stating 0-axis current";
  Vdc = 3*sqrt(3)/Modelica.Constants.pi*vdq "calculating vdc";
  id = -sqrt(3)*2/(Modelica.Constants.pi)*sin(theta)*Idc "d-axis current";
  iq = -sqrt(3)*2/(Modelica.Constants.pi)*cos(theta)*Idc "d-axis current";
  i0 = 0 "0-axis current";
```

Since this converter is not controllable, it means that the voltage regulation on its DC terminal can be indirectly controlled by the AC terminal's voltage amplitude. Therefore, if a constant DC-bus voltage is desirable, the six-pulse diode bridge should be associated with FCSG, which should have its own terminal voltage regulation. Then, this excitation system can be used control the DC bus voltage.

V. Modeling and Implementation of Controllers

A. Motor Control

A VSC is connected to the PMSM in order to control its speed. Considering that the PMSM is a surface-mounted motor, i.e. $L_d = L_q = L$, and considering that all states can be properly measured or estimated, it is possible to use a state feedback law. The control inputs of this model are the modulation indices of the VSC actuating as an inverter and are defined as in Equation (10).

$$\begin{cases} m_d = \dfrac{\kappa}{V_{DC}} \left[R_s i_d - L p \omega_m i_q - K_d L (i_d - I_d^*) \right], \\ m_q = \dfrac{\kappa}{V_{DC}} \left[R_s i_q + L p \omega_m i_d + p \omega_m \lambda_m - K_q L (i_q - I_q^*) \right]. \end{cases} \tag{10}$$

where K_{dq} is the control gain of dq coordinates, I^*_{dq} is the reference current for $dq-$axes and $\kappa = 2$ if the converter is half-bridge or $\kappa = \sqrt{3}$ if the converter is full-bridge. Furthermore, if Equation (10) is replaced in (7) and the terminal of the VSC is connected to the PMSM's terminal, that is, $v_{T,dq} = v_{dq}$, it is possible to simplify the motor's dynamic equations into the set presented in Equation (11).

$$\begin{cases} \frac{d}{dt} i_d &= -K_d(i_d - I^*_d), \\ \frac{d}{dt} i_q &= -K_q(i_q - I^*_q). \end{cases} \tag{11}$$

Note that K_d and K_q became the eigenvalues for i_d and i_q, respectively. In addition, if λ^*_d, T^*_L and ω^*_m are the nominal values for the $d-$axis magnetic flux, load torque and mechanical speed, respectively, it is possible to write that

$$I^*_d = \frac{\lambda^*_d - \lambda_m}{L}, \tag{12}$$

$$I^*_q = \frac{2}{3p\lambda_m}\left[T^*_L - K_\omega pJ\left(\omega_m - \omega^*_m\right)\right]. \tag{13}$$

If K_q is appropriately larger than K_ω, the $q-$axis controller is able to track the reference value I^*_q such that $T_L \approx T^*_L$ for all instants. Hence, it is possible to consider that the swing equation for the controlled model becomes (14). Therefore, all three states from the PMSM can be controlled via the the terminal voltages of the inverter.

$$\frac{d}{dt}\omega_m = \frac{3\lambda_m}{2J} I^*_q - \frac{T_L}{Jp} = -K_\omega\left(\omega_m - \omega^*_m\right). \tag{14}$$

The value for the gains used in this study are $K_d = K_q = 100$ while $K_\omega = 10$. Meaning that the current loop control is set to be approximately 10 times faster the speed loop control.

B. DC-Bus Voltage Control via Voltage-Sourced Rectifier

If a VSC is used to perform the interface between a PMSG and the DC bus, the converter is connected to the permanent magnet machine through a filter. This filter is, usually, an LCL filter but, if the capacitor is selected adequately, its dynamic behavior can be approximated to an RL branch [9]. Given this approximation, considering that reference currents flow out of VSC terminals, and that the system is in $dq-$frame, it is possible to write that [9, 12]:

$$\begin{cases} v_{T,q} - v_{s,q} = Ri_q + L\frac{di_q}{dt} + L\omega i_d, \\ v_{T,d} - v_{s,d} = Ri_d + L\frac{di_d}{dt} - L\omega i_q, \end{cases} \tag{15}$$

where $v_{s,d}, v_{s,q}$ are the voltages of the PMSG, R is the resistance and L is the inductance of the RL filter. If the reference currents flow from the PMSG into the VSC terminals, then the dynamics are given by

$$\begin{cases} L\frac{di_q}{dt} = -Ri_q - L\omega i_d + v_{s,q} - v_{T,q}, \\ L\frac{di_d}{dt} = -Ri_d + L\omega i_q + v_{s,d} - v_{T,d}. \end{cases} \tag{16}$$

As far as the control design is concerned, assume that all signals involved in the equation, i.e. $i_d, i_q, v_{d,s}, v_{q,s}, \omega$, are measured. Then VSC the terminal voltages can be designed to regulate i_d to i^*_d, and i_q to i^*_q. In fact, if the terminal voltages are given by

$$\begin{cases} v_{T,q} = -Ri_q - L\omega i_d + v_{s,q} + K_q L(i_q - I^*_q), \\ v_{T,d} = -Ri_d + L\omega i_q + v_{s,d} + K_d L(i_d - I^*_d), \end{cases} \tag{17}$$

then, Equations (16) can be re-written as

$$\begin{cases} L\dfrac{di_q}{dt} = -Ri_q - L\omega i_d + v_{s,q} - \left[-Ri_q - L\omega i_d + v_{s,q} + K_q L(i_q - I_q^*)\right], \\ L\dfrac{di_d}{dt} = -Ri_d + L\omega i_q + v_{s,d} - \left[-Ri_d + L\omega i_q + v_{s,d} + K_d L(i_d - I_d^*)\right], \end{cases} \tag{18}$$

which can be further simplified into

$$\begin{cases} \dfrac{di_q}{dt} = -K_q(i_q - I_q^*), \\ \dfrac{di_d}{dt} = -K_d(i_d - I_d^*). \end{cases} \tag{19}$$

The modulation corresponding to the terminal voltages in Eq. (17)

$$\begin{cases} m_q = \kappa\dfrac{v_{T,q}}{V_{DC}}, \\ m_d = \kappa\dfrac{v_{T,d}}{V_{DC}}. \end{cases} \tag{20}$$

Reference currents I_d^* and I_q^* can be calculated in an outer dynamic loop that can be designed for the control of voltage magnitude and DC capacitor voltage, for example. In this system, consider that no control over the AC terminal voltage of the PMSG is executed. Hence $I_d^* = 0$. In addition, the q-axis current reference can be calculated for controlling the DC bus voltage by using

$$I_q^* = \frac{2\kappa}{3m_q}\left[I_{DC} - K_v C_{DC}\left(v_{DC} - V_{DC}^*\right)\right]. \tag{21}$$

This last equation can be used by the outer loop to control the DC link voltage if some conditions are met. For example, the speed of the current loop should be much faster than the time constant governing the DC voltage dynamics. Hence, if $K_q, K_d >> K_v$ it is possible to write the following dynamics for the capacitor voltage

$$\begin{aligned} C_{DC}\frac{d}{dt}v_{DC} &= -\frac{3m_d i_d}{2\kappa} - \frac{3m_q i_q}{2\kappa} + I_{DC} = -\frac{3m_q I_q^*}{2\kappa} + I_{DC}, \\ &= -\frac{3m_q}{2\kappa}\frac{2\kappa}{3m_q}\left[I_{DC} - K_v C_{DC}\left(v_{DC} - V_{DC}^*\right)\right] + I_{DC}, \end{aligned} \tag{22}$$

which would result in the first order dynamics presented in Eq. (23).

$$\frac{d}{dt}v_{DC} = -K_v\left(v_{DC} - V_{DC}^*\right). \tag{23}$$

For this control system, $K_d = K_q = 250$ while $K_v = 50$, meaning that the current loop control is set to be approximately 5 times faster the DC bus loop control.

C. FCSG Terminal Voltage Control

The terminal voltage control of the FCSG is done by controlling the current that flows through the excitation field [13]. This is done indirectly, by controlling the voltage over the field circuit. In this study, the terminal voltage is compared to a reference value, that should be calculated in a way it ensures that the DC voltage output of the six-pulse diode bridge is kept constant in the desired value for a normal operation of the entire turboelectric system.

The basic dynamics behind the terminal voltage regulation is shown in the diagram depicted in Figure 6a. There, the reference terminal voltage is calculated via a simple gain applied to the DC bus voltage reference value. The resulting voltage is then compared with the measured machine's terminal voltage, and the error is applied to the regulator's control system. The resulting field voltage is the input to the field circuit that has the field current as output, affecting the terminal voltage through the generator equations [13, 14]. The excitation system highlighted in green in Figure 6a can be represented, for example, as a simplification of the IEEE type ST2A [15] without the load compensation branch

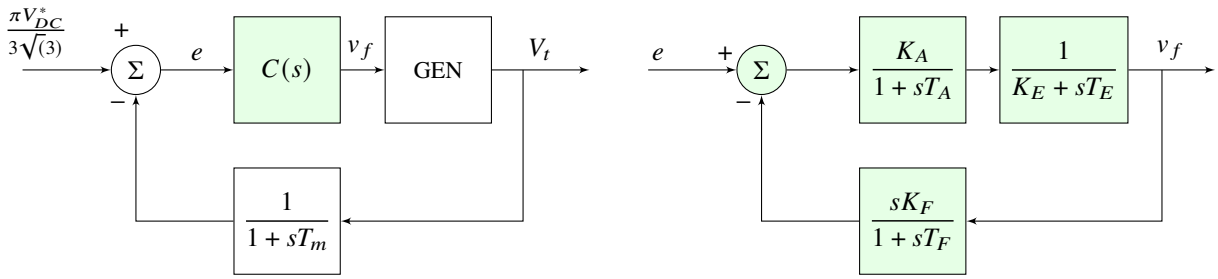

(a) Excitation and connection to generation. **(b) Excitation control system for the FCSG.**

Fig. 6 Simple diagram the excitation effect over the terminal voltage of the FCSG and its control system diagram.

or the inductance saturation effects. This system represents a static excitation system with a PEC that directly acts on the excitation field [13]. This excitation system is often employed in generators with large power ratings that need to comply with standard metrics for performance [16]. Hence, the system can represented by the diagram presented in Figure 6b.

The control system is implemented in Modelica using the diagram layer shown in Figure 7. Note that comparing the Modelica implementation and the diagrams displayed in Figure 6, there is one extra component that contributes to the variable e representing the error between the reference and measured values. This is due to the fact that exciters usually work with an amplification of the error, meaning that, in steady state, $v_f = \frac{K_A}{K_E} e$. Although K_A is usually very large, meaning that the error is indeed very small, the additional component compensates for such steady state error, making it zero during initial conditions. Another important observation that should be done is that excitation systems are often tuned using *per unit* values and, therefore, it is necessary to divide by the voltage base before the input e and then multiply by it after v_f.

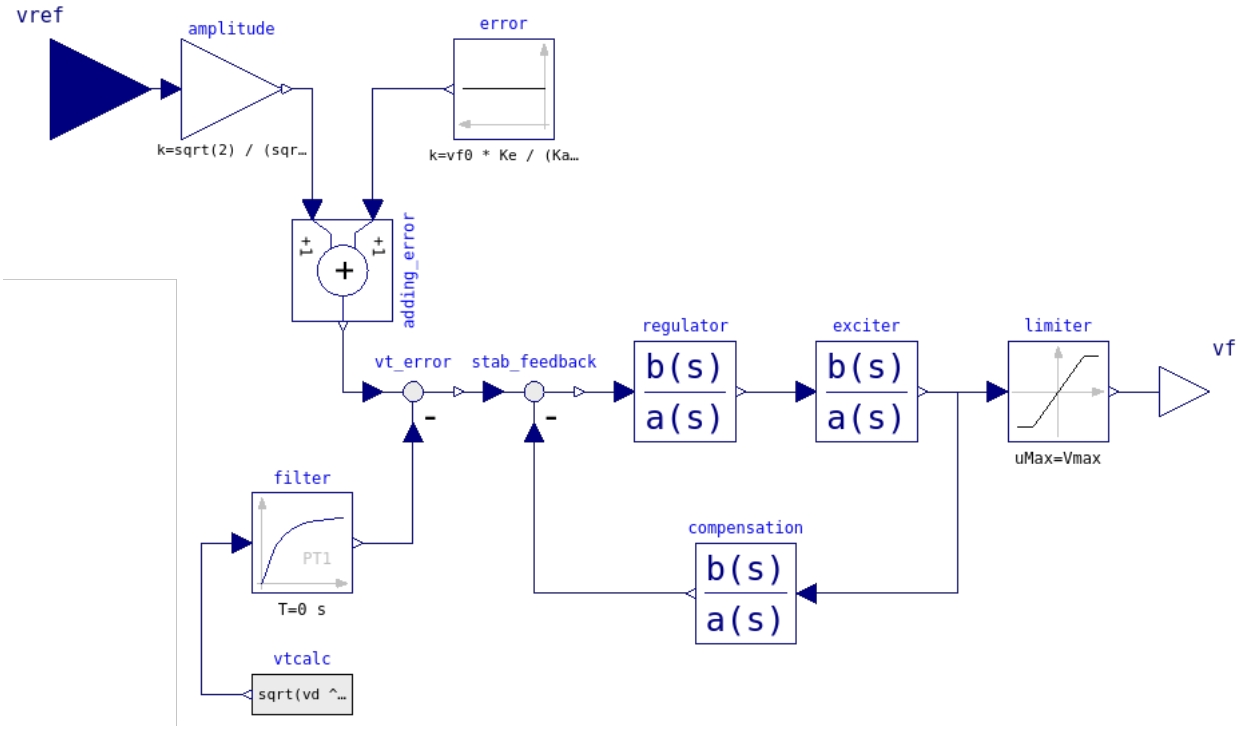

Fig. 7 Modelica implemntation of the excitation control system for the FCSG.

In this study, the parameters used in terminal voltage control for the FCSG are displayed in Table 1.

Table 1 Synchronous Generator Excitation System Parameters

Parameter	Description	Value	Unit
T_m	Measurement time constant	0.5	ms
K_A	Regulator gain	200	V/V
T_A	Regulator time constant	0.02	s
K_f	Stabilizer compensator derivative gain	0.001	s
T_f	Stabilizer compensator time constant	0.82	s
K_e	Exciter constant	1	V/V
T_e	Exciter time constant	0.021	s

VI. Flight Mission Profile Modeling

The flight mission profile is implemented in this study by the use of reference curves for speed, in the turbine side, and for speed and torque at the fan's side. The profile considers an example flight mission of 400 seconds and the reference curves are shown in Figure 8.

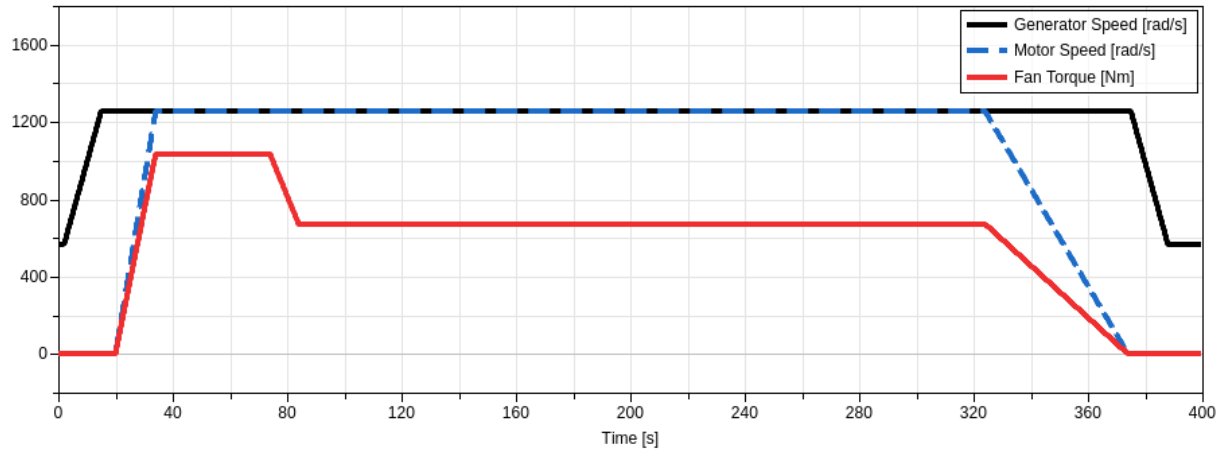

Fig. 8 Flight mission load profile for the electrical motor in terms of torque, speed and for the electrical generator in terms of speed.

First, let us look at the turbine side or, in other words, let us look at the dark solid curve. At the beginning, the generator is considered to be already spinning at its lowest nominal value of 5400 rpm or 360 Hz in the electrical frequency. At $t = 2s$ the turbine is set to increase its speed, leading the electrical generator to increase its frequency to 800 Hz as in preparation for the take-off. This ramp-up procedure takes 13 seconds. After that, the generator's speed is maintained at a constant until $t = 375$ seconds. After the entire flight mission is performed, the generator's speed reference decreases to the 5400 rpm again, taking up 13 seconds and remaining at that value until the end of the simulation.

Now, looking at the fan side, there are two different curves, speed and torque. The curve in dashed blue is the motor's speed reference and it starts to increase at $t = 20$ seconds until it reaches the nominal speed of 5400 rpm. This process takes 14 seconds and is used to represent the *take-off*. After that, during *climb* and *cruise*, the speed is maintained constant at 5400 rpm. Finally, at $t = 330$ seconds, the *descent and landing* part begins and the speed starts diminishing until it reaches 0, at $t = 380$ seconds. The fan torque curve, in solid red, also starts to increase at $t = 20$ seconds until it reaches its maximum value of 1035 Nm, representing the *take-off* and taking 14 seconds. For the *climb* period, the torque remains at its maximum value for 40 seconds. After that, the torque diminishes until it reaches 65% of its maximum value, which is the torque needed for the *cruise*. It remains at this value for 240 seconds, until it reaches $t = 330$ seconds, when the *descent and landing* part begins, reducing the torque to zero and taking 50 seconds.

VII. Studied Turboelectric Architectures

Two different examples of turboelectric systems are analyzed in this paper and their differences arise from the distinctive adoption of "Electrical Generator" and "AC/DC Converter", from Figure 1. The turbine and the fan (load) are all represented by sources of torque in Modelica, being directly influenced by the flight mission profile described in the previous section. However, it is important to notice that the developed models allow these torque sources to be replaced by detailed models of these mechanical components. In all four cases, the generator is considered to be connected to the turbine via a gearbox with a fixed ratio, instead of a Constant Speed Drive (CSD), to reduce the complexity of the mechanical system, following the practice adopted in the latest aircraft models like the Boeing 787 and the Airbus 380 [17]. Therefore, in all four cases, the generator operates under a Variable Speed Variable Frequency (VSVF) regime, meaning that the system's frequency changes proportionally to the engine's speed [1].

A. DC Link, Inverter and Motor

This part is similar in both studied architectures and, therefore, it is worth it to describe it separately. The DC link is composed by a capacitor with $C = 47\ \mu$F and a resistor $r_{DC} = 10$ mΩ used to represent cable thermal losses. The voltage value over the DC capacitor is different in each architecture due to the different adopted AC/DC converters and therefore, it will be specified in their own dedicated subsections. The VSI uses the control system and the parameters described in Subsection V.A and the parameters for the PMSM used in both architectures are described in Table 2.

Table 2 Permanent Magnet Synchronous Motor Parameters.

Parameter	Description	Value	Unit
r_s	Stator resistance	0.051	Ω
L_q	Quadrature axis inductance	0.5	mH
L_d	Direct axis inductance	0.5	mH
L_0	Zero axis inductance	0.5	mH
λ_m	Permanent magnet flux	0.46	Wb
J_M	Motor's moment of inertia	2.88	$Kg \cdot m^2$
ω_n	Nominal speed	$360 - 800$	Hz
p	Number of pairs of poles	4	–

B. Studied Architecture 1: PMSG and VSC

The first configuration has a PMSG as its electrical generator and a VSC acting as a rectifier. The reason behind this choice lies in the fact that PMSG has high efficiency and power density, therefore becoming advantageous to consider in such turboelectric architectures [6, 18]. The VSC is chosen due to its capability of DC bus voltage control by regulation of the modulation indices, as shown in Subsection V.B. These two components are interconnected via an RL filter, used to smooth the currents into almost-sinusoidal waves and, therefore, avoid jeopardizing the generator's expected performance due to possible harmonics. The Modelica diagram for this configuration is presented in Figure 9, where the electrical system together with its controllers and torque sources are all represented.

The RL filter that is used to interface the PMSG and the VSC acting as a rectifier has resistance $r = 0.1$ mΩ and inductor $L = 0.1$ mH. Besides that, the voltage over the DC link capacitor is 6 kV, which is much higher than the current practices. However, the adopted values are well suited for a much higher power demand, which could be adopted on turboelectric architectures due to, for example, higher efficiency in such high power levels [6, 19, 20]. The VSC, which is connected in full-bridge architecture (i.e. $\kappa = \sqrt{3}$), is controlled using the strategy presented in Subsection V.B, using the $K_d = K_q = 250$ and $K_v = 50$. The PMSG parameters are summarized on Table 3 below.

C. Studied Architecture 2: FCSG and Diode Bridge

In the second system, the PMSG is replaced by the FCSG, which has its field current being controlled in order to guarantee that the terminal voltage is kept in its nominal value. Therefore, the FCSG is composed by a three stage machine [2] and the field current control system. Since the terminal voltage is controlled, the DC voltage is not expected to present large variations when a 6-pulse diode bridge is used as a rectifier. The diagram for this architecture is

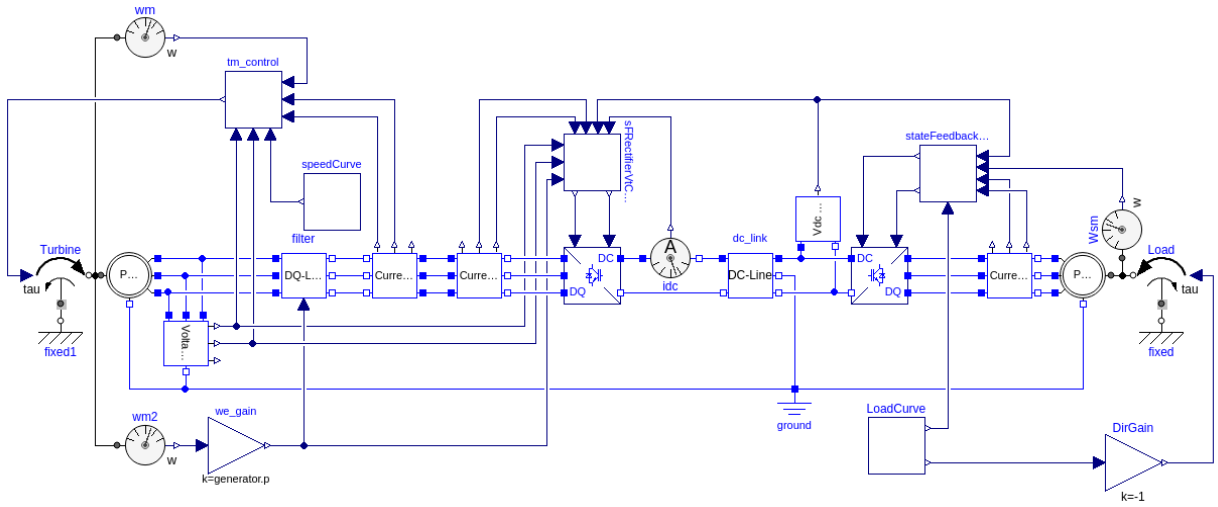

Fig. 9 Modelica implementation of the studied turboelectric systems with PMSG and VSC as rectifier.

Table 3 Permanent Magnet Synchronous Generator Parameters

Parameter	Description	Value	Unit
R_s	Stator resistance	0.076	Ω
L_q	Quadrature axis inductance	0.8	mH
L_d	Direct axis inductance	0.8	mH
L_0	Zero axis inductance	0.8	mH
λ_m	Permanent magnet flux	0.56	Wb
J_G	Generator's moment of inertia	2.68	$Kg \cdot m^2$
ω_n	Nominal speed	360 – 800	Hz
p	Number of pairs of poles	4	–

presented in Figure 10. Note that, in this case, because the diode rectifier is used, the nominal voltage for the DC bus is 3 kV.

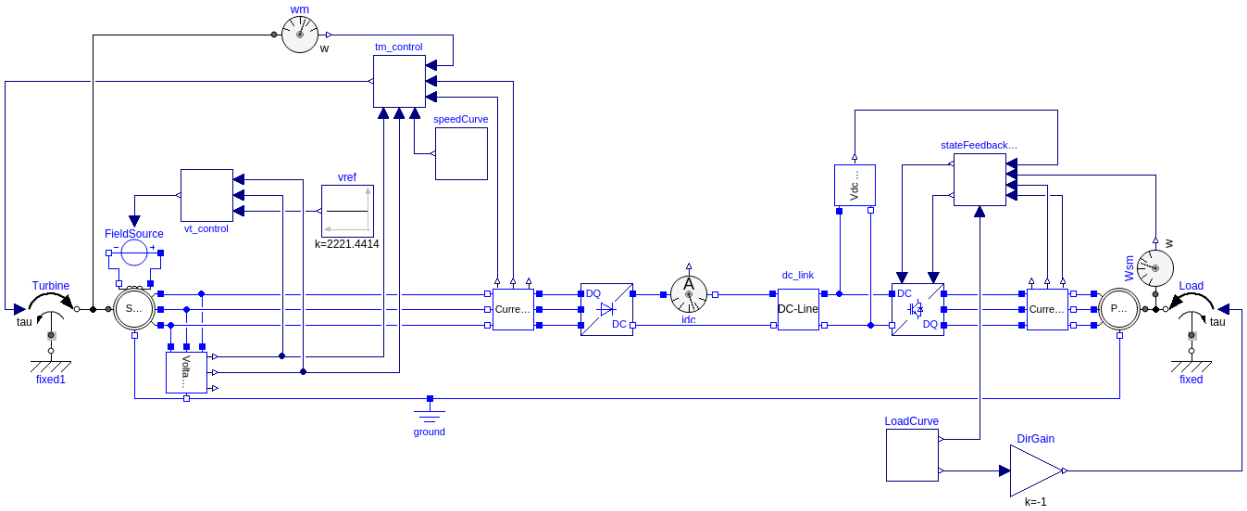

Fig. 10 Modelica implementation of the studied turboelectric systems with FCSG and diode bridge as rectifier.

The terminal voltage control is performed using the circuits and the parameters present in Subsection V.C. The parameters for the FCSG are summarized on Table 4.

Table 4 Field Controlled Synchronous Generator Parameters

Parameter	Description	Value	Unit
r_f	Field circuit resistance	0.076	Ω
L_f	Field circuit inductance	45	mH
r_s	Stator resistance	0.076	Ω
L_{ls}	Stator inductance	0.3	mH
L_{mq}	Quadrature axis magnetizing inductance	0.5	mH
L_{md}	Direct axis magnetizing inductance	0.5	mH
r_{kdq}	D and Q axes damping resistance	0.5	$m\Omega$
L_{kdq}	D and Q axes damping inductance	0.15	mH
J_G	Generator's moment of inertia	2.68	$Kg \cdot m^2$
ω_n	Nominal speed	$360 - 800$	Hz
V_t	Generator's terminal voltage (nominal)	2220	V
p	Number of pairs of poles	4	–

VIII. Simulation Results

The simulation results presented in this section correspond to a 400−second simulation in Dymola, using the variable time-step DASSL solver [21], with tolerance equal to 10^{-6} and displaying 50 thousand points for each output curve. Architecture 1 has 565 DAE equations and unknowns and its simulation took 7.81 seconds, while Architecture 2 is compiled with 518 DAE scalar unknowns and equations and it took 2.23 seconds to simulate.

A. Architecture 1:PMSG and VSC

The results for the variables related to the PMSG are depicted in Figure 11. Note that, since the control acting on the VSC is acting only to keeping $d-$axis current equal to zero and the DC-link voltage constant, the generator's terminal voltage, i.e. $\sqrt{v_d^2 + v_q^2}$, actually increases when the generator's speed increases. Recall that there is no excitation field control in a permanent-magnet-type machine. The lack of control for the generator's terminal voltage makes it difficult for other devices to be connected in the AC bus close to the generator but note that adequate reference values for $d-$axis current could ensure the generator's terminal voltage to be constant.

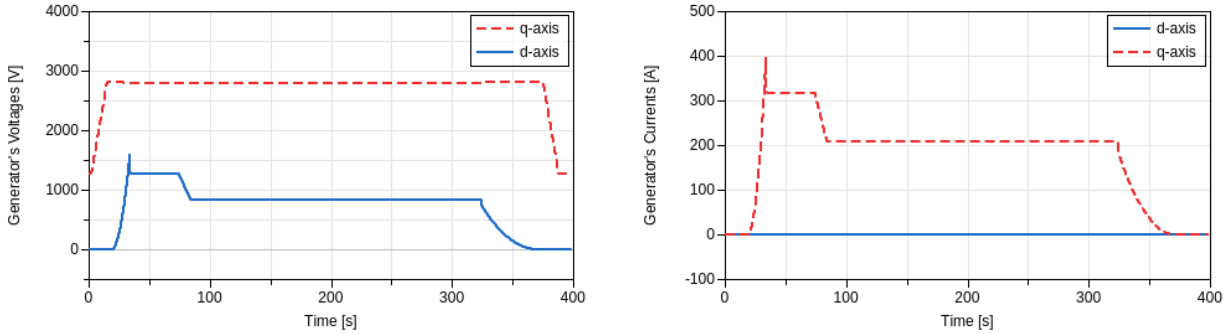

(a) Terminal voltages on PMSG. **(b) Terminal currents on PMSG.**

Fig. 11 Resulting PMSG terminal $dq-$frame currents and voltages.

The DC bus voltage is controlled by $q-$axis current from the inverter and, as it is presented in Figure 12a, this task

can be done properly during the simulated flight mission. Note that the DC bus voltage varies less than 1% during the entire simulation. In addition, the motor currents are depicted in Figure 12b and it is possible to note similarities between $q-$axis currents from Figure 11b. This is because both AC systems are coupled in terms of active power, which could be controlled by $q-$axis current. However, the different behavior observed on $d-$axis current shows the decoupling between the two AC systems allowed by the AC/DC/AC configuration of the turboelectric architecture studied here.

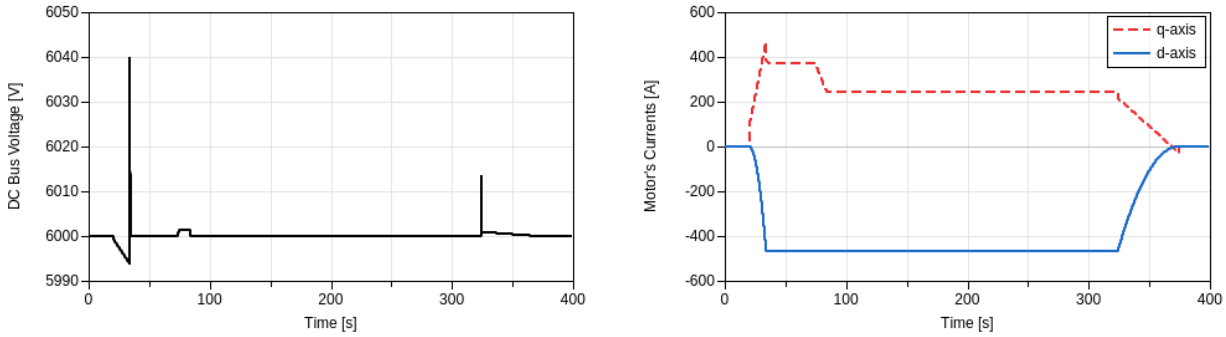

(a) Controlled DC bus voltage. **(b) PMSM terminal currents.**

Fig. 12 DC bus voltage and terminal currents for permanent magnet motor for Architecture 1.

B. Architecture 2:

The results for the FCSG variables are presented in Figure 13. Note that, in this case, the $q-$axis current is not controlled to be zero and, therefore, it varies differently from what is presented in Fig. 11b. Note also that the voltage over the field circuit varies in order to keep the generator's terminal voltage constant throughout the flight mission, therefore, making the DC bus voltage to be constant as well.

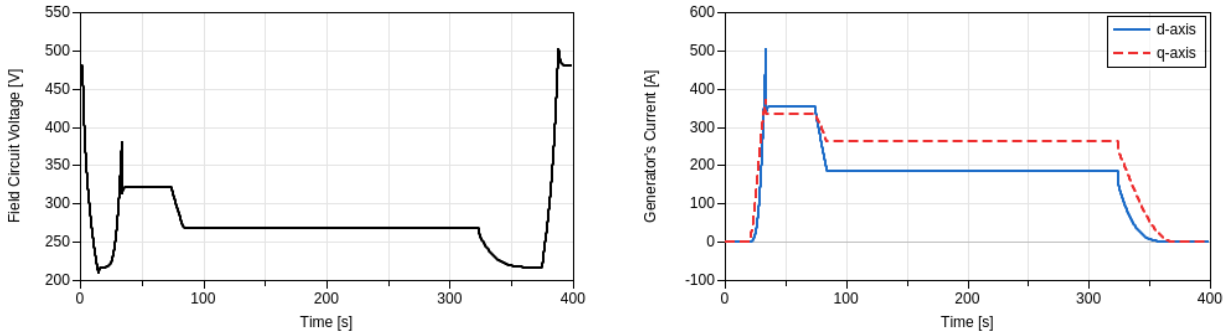

(a) Field circuit voltage on FCSG. **(b) Terminal currents on FCSG.**

Fig. 13 Resulting FCSG field circuit voltage and terminal $dq-$frame currents.

The DC-bus voltage resulting from the simulation of the second architecture is presented in Figure 14a. Note that the voltage varies around 4% in the worst case scenario and, therefore, the terminal voltage control can be considered to be successful. It is also important to highlight that different controllers can be additionally designed in order to improve this dynamic performance. The motor currents for this architecture are depicted in Figure 14b and it is possible to note that they are very similar to the results presented in Figure 12b, showing once again that, if variables are properly controlled, the performance of one side of the system does not affect the other. In this case, it is shown how the motor performance is almost independent from the type of generator and its controller as long as the DC bus voltage is properly controlled.

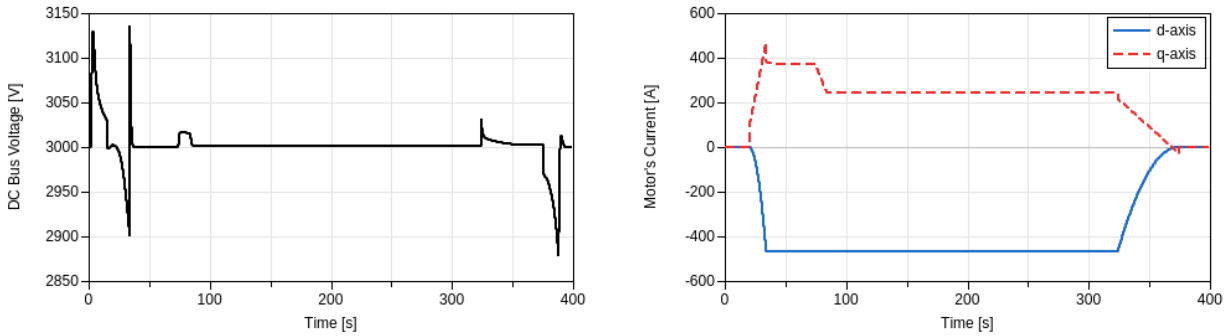

(a) Controlled DC bus voltage. **(b) PMSM terminal currents.**

Fig. 14 DC bus voltage and terminal currents for permanent magnet motor for Architecture 2.

IX. Conclusion

This paper provides the dynamical models of various electrical devices, from synchronous machines to power electronic converters, in $dq-$frame, along with different controllers that are used to regulate these devices' dynamic behavior and their implementation in Modelica language. The choice for the $dq-$frame allows fast dynamic simulation and analysis of relatively complex turboelectric propulsion architectures to be made. In addition, other simplifications occur when the $dq-$frame is adopted such as in control implementation. In result, it was shown that even the simulation of $400-$second flight mission took, at most, 7.81 seconds to be simulated. The current paper illustrates how Modelica can be done to study turboelectric architectures that are necessary for the development of more electric aircrafts.

This paper also shown that transient stability performance must be taken into account when sizing the system and defining its parameters. For example, different DC voltages had to be implemented in the different turboelectric architectures due to the converter type that is used. Furthermore, it is possible to highlight challenges and strengths from studied each architecture. For instance, configurations with PMSG are lighter than the FCSG case, although they require more complicated power electronics converter to regulate DC bus voltage. On the other hand FCSG architectures allow the regulation of the generator's terminal voltage and DC bus voltage at their desired values with simpler rectifier but the terminal voltage control might be more challenging and, if poorly designed, the controllers can lead the entire system to instability.

Because of that, future works include the analysis of better control strategies for different architectures, including more realistic models for turbine and fan. Furthermore, it is also important to study noise applied to the flight mission profile and its effects over the architecture dynamic performance.

References

[1] Sarlioglu, B., and Morris, C. T., "More electric aircraft: Review, challenges, and opportunities for commercial transport aircraft," *IEEE transactions on Transportation Electrification*, Vol. 1, No. 1, 2015, pp. 54–64.

[2] Bozhko, S., Hill, C. I., and Yang, T., "More-Electric Aircraft: Systems and Modeling," *Wiley encyclopedia of electrical and electronics engineering*, 2018, pp. 1–31.

[3] Hall, D. K., Huang, A. C., Uranga, A., Greitzer, E. M., Drela, M., and Sato, S., "Boundary layer ingestion propulsion benefit for transport aircraft," *Journal of Propulsion and Power*, Vol. 33, No. 5, 2017, pp. 1118–1129.

[4] Kratz, J. L., and Thomas, G. L., "Dynamic analysis of the STARC-ABL propulsion system," *AIAA Propulsion and Energy 2019 Forum*, 2019, p. 4182.

[5] Gohardani, A. S., Doulgeris, G., and Singh, R., "Challenges of future aircraft propulsion: A review of distributed propulsion technology and its potential application for the all electric commercial aircraft," *Progress in Aerospace Sciences*, Vol. 47, No. 5, 2011, pp. 369–391.

[6] Benzaquen, J., He, J., and Mirafzal, B., "Toward more electric powertrains in aircraft: Technical challenges and advancements," *CES Transactions on Electrical Machines and Systems*, Vol. 5, No. 3, 2021, pp. 177–193.

[7] Bals, J., Ji, Y., Kuhn, M. R., and Schallert, C., "Model based design and integration of more electric aircraft systems using modelica," *Moet forum at European power electronics conference and exhibition*, 2009, pp. 1–12.

[8] Bogodorova, T., Sabate, M., Leon, G., Vanfretti, L., Halat, M., Heyberger, J.-B., and Panciatici, P., "A modelica power system library for phasor time-domain simulation," *IEEE PES ISGT Europe 2013*, IEEE, 2013, pp. 1–5.

[9] Yazdani, A., and Iravani, R., *Voltage-sourced converters in power systems: modeling, control, and applications*, John Wiley & Sons, 2010.

[10] Kassakian, J. G., Schlecht, M. F., and Verghese, G. C., *Principles of power electronics*, Vol. 1991, Addison-Wesley Reading, MA, 1991.

[11] Finotti, C., Gaio, E., Benfatto, I., Song, I., and Tao, J., "Continuous state-space model in dq frame of the thyristor AC/DC converters for stability analysis of ITER pulsed power electrical system," *IEEE Transactions on Plasma Science*, Vol. 44, No. 11, 2016, pp. 2923–2931.

[12] Krause, P. C., Wasynczuk, O., Sudhoff, S. D., and Pekarek, S. D., *Analysis of electric machinery and drive systems*, Vol. 75, John Wiley & Sons, 2013.

[13] Kundur, P., *Power system stability and control*, CRC press New York, NY, USA, 2007.

[14] Chapman, S. J., *Electric machinery fundamentals*, McGraw-Hill, 2004.

[15] *IEEE Recommended Practice for Excitation System Models for Power System Stability Studies*, IEEE Standard 421.5, 1992.

[16] Nøland, J. K., Nuzzo, S., Tessarolo, A., and Alves, E. F., "Excitation System Technologies for Wound-Field Synchronous Machines: Survey of Solutions and Evolving Trends," *IEEE Access*, Vol. 7, 2019, pp. 109699–109718.

[17] Wang, Y., Nuzzo, S., Zhang, H., Zhao, W., Gerada, C., and Galea, M., "Challenges and opportunities for wound field synchronous generators in future more electric aircraft," *IEEE Transactions on Transportation Electrification*, Vol. 6, No. 4, 2020, pp. 1466–1477.

[18] Zhang, X., Bowman, C. L., O'Connell, T. C., and Haran, K. S., "Large electric machines for aircraft electric propulsion," *IET Electric Power Applications*, Vol. 12, No. 6, 2018, pp. 767–779.

[19] Zhang, D., He, J., and Pan, D., "A megawatt-scale medium-voltage high-efficiency high power density "SiC+ Si" hybrid three-level ANPC inverter for aircraft hybrid-electric propulsion systems," *IEEE Transactions on Industry Applications*, Vol. 55, No. 6, 2019, pp. 5971–5980.

[20] He, J., Zhang, D., and Torrey, D., "Recent advances of power electronics applications in more electric aircrafts," *2018 AIAA/IEEE Electric Aircraft Technologies Symposium (EATS)*, IEEE, 2018, pp. 1–8.

[21] Petzold, L. R., "Description of DASSL: a differential/algebraic system solver," Tech. rep., Sandia National Labs., Livermore, CA (USA), 1982.